Soft Matter

PAPER

View Article Online
View Journal | View Issue

Cite this: *Soft Matter*, 2021, **17**, 1861

Soft cavitation in colloidal droplets

Myrthe A. Bruning, *[a] Claus-Dieter Ohl[b] and Alvaro Marin *[a]

Received 10th November 2020,
Accepted 10th December 2020

DOI: 10.1039/d0sm02002h

rsc.li/soft-matter-journal

When a pure droplet evaporates inside an elastic medium, two instabilities are typically observed. As the droplet shrinks, the elastic medium needs to deform and elastic tension builds up. At a critical strain, accumulated tension at the gel–droplet interface is released by developing creases. The droplet keeps shrinking beyond this point, pulling the elastic network and therefore decreasing the pressure in the liquid phase. This drives the liquid phase into a metastable state, and leads to the second instability: the nucleation of a vapour bubble in the liquid phase by cavitation. These instabilities consistently occur in the described order whenever a pure liquid (water, in this case) is used. The presence of colloidal particles inside droplets is common both *in vitro* and in natural environments, and they can change such phenomenology significantly by stimulating cavitation events before any creasing instability. In this work, we study the role of colloidal particle size and concentration on the early inception of cavitation in water droplets in an elastic medium. Our results reveal an unexpected dependence with the particle size and with the size distribution of the colloidal particles. Given the simplicity and reliability of the system and preparation, the method described here could be eventually used to measure tensile strengths of particle solutions with accuracy.

1 Introduction

Soft materials and surfaces develop complex instabilities under dehydration, typically wrinkling and creasing.[1,2] Such evaporation-driven instabilities are visible in our everyday life at the milk surface[3] or even in our human skin.[4] Another type of evaporation-driven instability that might occur during dehydration is cavitation, the sudden emergence and expansion of a bubble within a liquid phase subjected to a negative hydrostatic stress. For such instability to occur, liquid inclusions must be present within a soft (or hard) solid undergoing tension. Many examples can be found in nature. In the mineral kingdom, droughts can induce negative stresses in porous soils, giving rise to cavitation events and altering the soil structure.[5,6] Among the examples that can be found in the plant kingdom are the xylem embolia, which are caused by cavitation events during the droughts in summer,[7] and the spectacular fern sporangium[8] which makes use of cavitation events within its cells to disperse its spores through the air.

In laboratory conditions, this combined phenomenon of evaporation and cavitation has been studied both for laser-generated cavities inside water-soaked hydrogels[9–11] and for water droplets inside silicone-based gels.[2,12] Interestingly, in the latter case, given the permeability of polydimethylsiloxane (PDMS) for water vapour, it has been shown[2,12] that the evaporation of a water droplet occurs following a simple diffusion-limited process, retaining its spherical shape for most of its lifetime. However, after reducing its radius a certain critical fraction (which depends on the properties of the elastic medium), the gel–liquid interface displays a so-called creasing instability.[2] The interface folds onto itself, in order to release part of its tension which builds up during the shrinkage of the droplet. As the droplet keeps evaporating after creasing, the tension in the elastic medium keeps increasing, introducing a negative pressure inside the water droplet. As a result, the droplet suffers a cavitation event and a bubble nucleates, which eventually grows up to the same size as the initial droplet. The fast dynamics and oscillations of this bubble have been studied in detail recently.[12] It is worth noting that the phenomenon is so reproducible, that the frequency of these oscillations could serve as a proxy of the viscoelastic properties of the surrounding gel.[11]

Water in soil or inside xylem channels typically contains impurities that can alter this phenomenology significantly. By sending a shock-wave to a particle solution, Borkent *et al.*[13] confirmed experimentally that the presence of particles can trigger the formation of bubbles at lower tension levels than those predicted for pure water. Their results confirmed the crevice model for cavitation nuclei,[14] which modelled and quantified the energy needed for the nucleation and growth of a bubble in a pre-existing cavity. In their experiments, particle surface roughness facilitated the entrapment of gas pockets and enhanced the chances of a cavitation event. Similar

[a] *Physics of Fluids Group, Faculty of Science and Technology, Mesa+ Institute, University of Twente, 7500 AE Enschede, The Netherlands. E-mail: m.a.bruning@utwente.nl, a.marin@utwente.nl*
[b] *Soft Matter & Cavitation Lab, Otto-von-Guericke University, Magdeburg, Germany*

phenomena have been observed when studying foaming upon beer tapping,[15] which occurs when the top of a beer bottle is hit with a solid object, usually another bottle, triggering violent foaming and spoiling the subject's drink. Interestingly, foaming in beer is facilitated by cellulose fibres that take the role as cavitation nuclei.[16] Besides the roughness of the particles, also their size is an important factor, as shown by Marschall *et al.*[17] They showed that cavitation nuclei are related to the fine scale structure of the particle surface. Critical cavities are developed, which depend on the global radii of curvature of the particle.

Experiments inside soft elastic media with evaporating pure liquid droplets have nearly always shown creasing instabilities preceding cavitation.[2,12] However, creasing has been rarely observed in natural conditions.[6,18] Motivated by this observation, in this work, we will introduce a known concentration of well-characterized colloids inside an evaporating water droplet in elastomer gels (PDMS) and study the effect of such "controlled impurities" on the instabilities observed: creasing and cavitation. The expectation is that the presence of impurities, *i.e.* colloidal particles in our case, will always promote cavitation before any creases are developed, which would explain why creasing is never observed in nature.

2 Experiments

In a typical experiment, a suspension droplet injected into an elastic medium is recorded as it evaporates and manifests cavitation and/or creasing instabilities. The gel used is Dow Corning polydimethylsiloxane (PDMS) Sylgard184 mixed in a 1 : 10 ratio (curing agent : base polymer). The static shear modulus μ_0 of this gel is $\sim$0.7 MPa. The experimental protocol involves mixing and degassing this gel and injecting the droplet after it has been cured for some time. In order to ensure similar conditions for each experiment, all of these steps follow a precisely timed protocol. After combining the curing agent and base polymer, the mixture is stirred for 2 minutes, and directly afterwards degassed in a vacuum chamber for 35 minutes. Within 5 minutes of releasing the vacuum, the gel is put in the experimental chamber. In this chamber the relative humidity is kept at 30% and the temperature of the bottom plate is 70 °C. The gel mix is poured in a transparent plastic box of dimensions 2.5 × 2.5 × 1.5 cm (width × depth × height) which is open at the top. This box is heated for 19 minutes after which the colloidal droplet will be inserted in the centre of the gel-filled box. By the time the droplet is injected, the gel is precured and the droplet stays where it is initially injected. Throughout the entire experiment the sample is heated at 70 °C. A schematic overview of the set-up is given in Fig. 1a.

The suspension consists of Milli-Q water with polystyrene colloidal particles, functionalized with sulfate groups, which makes the particles hydrophilic and conveys enough electrostatic repulsion between them to maintain the suspension stable with no need of additional stabilizers (microParticles GmbH, PS-FluoRed).

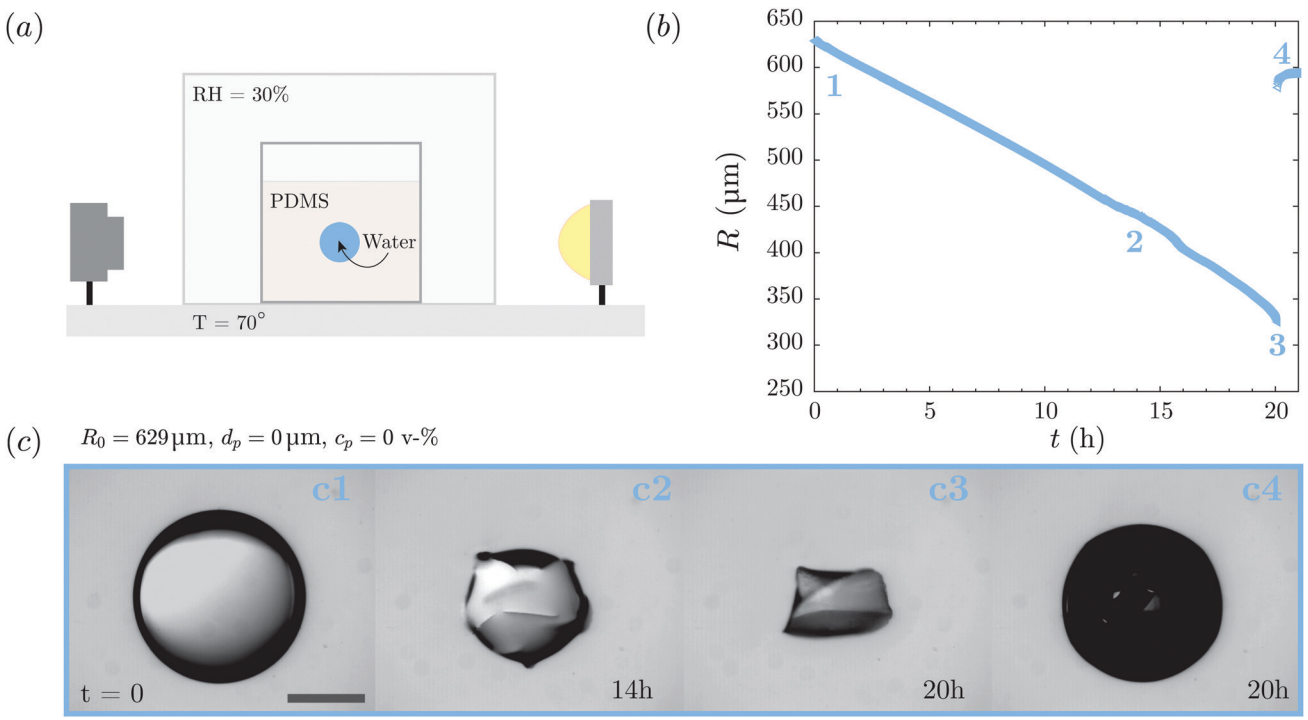

Fig. 1 Overview of the experimental set up and typical images that are captured. (a) A schematic representation of the set up, including the humidity controlled chamber and the temperature controlled bottom plate (not to scale). The droplet size is typically R_0 = 200–700 μm and contains different concentrations of polystyrene particles. Figures (b) and (c) are the evolution of the droplet radius as a function of time and the corresponding images, in this case for a pure water droplet. Panel c1 shows the initial (spherical) droplet, panel c2 the creasing instability and panels c3 and c4 are captured right before and after cavitation occurred. The scale bar in panel c1 represents 500 μm.

Two different particle sizes are used for the experiments (d_p = 0.45 ± 0.009 and 0.98 ± 0.04 μm) and three different particle concentrations (c_p = 0.15, 1 and 2.5 v%). The density of these particles is 1.05 g cm^{-3}, which makes them almost neutrally buoyant. Nonetheless, the duration of the experiment (up to 25 hours) can eventually be comparable to the time required for a colloidal particle to settle at the bottom of the droplet. This is indeed the case of our larger particles, as we will discus below. In order to prepare the suspensions, the stock solution is sonicated for 15 minutes prior to diluting. After preparing the desired volume concentration, the solution is sonicated for another five minutes to ensure no particle clusters are present. Droplets of these colloidal suspensions are injected using an Eppendorf pipette and range from 0.03–1.4 μl (meaning R_0 = 200–700 μm). The experiments are recorded using a Ximea MQ013MG-ON and frames are captured every minute. Experiments last from 2 to 25 hours depending on the initial droplet radius R_0. The camera is mounted outside the chamber and takes side view images of the droplet. From these recordings we can extract the (effective) droplet radius of the droplet and observe the appearance of creasing and cavitation.

The shrinkage of the droplet is shown in Fig. 1b, in which we show the radius as a function of time. Eventually, the radius shoots up to nearly its original value. As described extensively in ref. 12, this final event corresponds to the nucleation of a bubble through a cavitation event. During the evaporation of the droplet, the tension in the gel increases, which reduces the pressure inside the droplet. The liquid phase is then in a metastable state, sensitive to a cavitation event. Images for a typical experiment using pure water are shown in Fig. 1c. First, a spherical droplet is injected and starts to evaporate. At some point the elastic medium creases and the droplet looses its spherical shape (see panel c2, after 14 hours from injection). From that point onwards we determine the droplet size as an effective radius using its projected area. Finally, cavitation occurs and a bubble nucleates, which eventually grows up to a similar size as the initial droplet (panel c4).

3 Results

3.1 Diffusive droplet evaporation

As shown previously in the literature,[2,12] pure water droplets evaporate inside such gels following a diffusion-limited process. In Fig. 2 we compare the evaporation of colloidal droplets with the evaporation of a pure water droplet. To obtain an analytical form of the droplet radius R as a function of time, we start with a mass balance of the droplet in a diffusion-limited process:

$$\rho_w \frac{dV}{dt} = -4\pi R^2 J, \tag{1}$$

in which ρ_w is the water density. The volume of the droplet V can be expressed as $\frac{4}{3}\pi R^3$, $J = J(R)$ represents the diffusive flux at the droplet's interface $r = R$. This flux is given by Fick's law as

$$J = -D\frac{\partial C}{\partial r}\Big|_{r=R}, \tag{2}$$

which allows us to rewrite eqn (1) to

$$\rho_w 4\pi R^2 \frac{dR}{dt} = 4\pi R^2 D\frac{\partial C}{\partial r}\Big|_{r=R}. \tag{3}$$

The characteristic diffusion time scale is defined as $t_D = R_0^2/D = \mathcal{O}(10^2)$ s,[19] using R_0 = 600 μm and the diffusivity of water vapor in PDMS $D = 3.3 \times 10^{-9}$ m^2 s^{-1}.[20] We can express the typical droplet evaporation time as $t_F = R_0^2\rho_w/(2D\Delta c) = \mathcal{O}(10^5)$ s, which includes the density of water (ρ_w = 998 kg m^{-3}) and the concentration gradient at the interface and the far field (Δc = 33 mol m^{-3} [21]). As the diffusion time scale t_D is much smaller than the typical evaporation time t_F, the evaporation can be assumed to follow a steady-state solution:

$$\frac{\partial C}{\partial t} = \frac{D}{r^2}\frac{\partial}{\partial r}\left(r^2\frac{\partial C}{\partial r}\right) \approx 0. \tag{4}$$

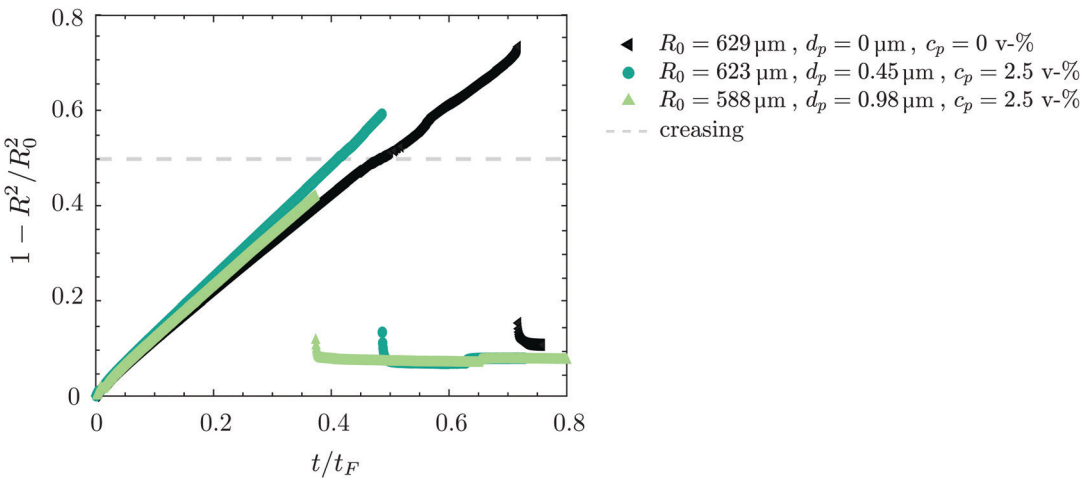

Fig. 2 The dimensionless droplet area loss as a function of dimensionless time while evaporating inside an elastic media for different particle sizes. The grey dotted line represents the dimensionless area at which creasing occurs for this elastic medium. The black markers represent the case of a pure water drop.

The final expression for the droplet radius reads as

$$R_0^2 - R(t)^2 = \frac{2D\Delta c t}{\rho_w}. \quad (5)$$

Using the expression for the typical evaporation time t_F, the final dimensionless equation for the droplet area loss in the case of steady-state diffusion is given by

$$1 - \frac{R(t)^2}{R_0^2} = t/t_F. \quad (6)$$

In Fig. 2 the typical evolution of the droplet radius, using eqn (6), is shown for different particle sizes. As a reference we also include an experiment without any particles present. From these curves we can see that the addition of particles to the droplet does not alter its evaporation: it follows the same curve as the pure water droplet. Initially this occurs in an isotropic manner and the droplet reduces its size holding its spherical shape. However, at a certain ratio for R/R_0 creasing occurs and the gel starts to fold onto itself. For this type of gel, $R_{crease}/R_0 = 0.71$, as observed both for pure water drops and colloidal drops. In a previous study,[12] we found experimentally a ratio of 0.73 for the same type of gel. The small discrepancy could be due to small differences in composition between different batches of gel. In Fig. 2 the radius of creasing is highlighted with a grey dotted line ($1 - R^2/R_0^2 = 1 - 0.71^2 = 0.5$). For some curves a small bend is observed after creasing occurs, because the droplet has lost its spherical shape. At some point, a cavitation event takes place and a bubble forms. As shown in Fig. 2, cavitation happens after the droplet has creased, both in the case of a pure water drop and for the smallest particle size used of diameter $d_p = 0.45$ μm. This picture changes dramatically for the droplets containing the largest particles ($d_p = 0.98$ μm), a large majority of them cavitates before the interface has creased. By doing so, creasing is completely suppressed since cavitation kicks in earlier, vaporizing the liquid phase. Consequently, we will refer to this situation as early cavitation.

This result raises several questions as, why do small particles not show this early cavitation? Does particle concentration play a role? Since the maximum tension (negative pressure) achievable is proportional to the initial droplet size, does it play a significant role? We will try to address these questions in the following.

3.2 Suppressing creasing

To study this phenomenon in more detail, Fig. 3 shows the difference between early cavitation and cavitation after creasing. The three cases shown in the sequences in Fig. 3 correspond to

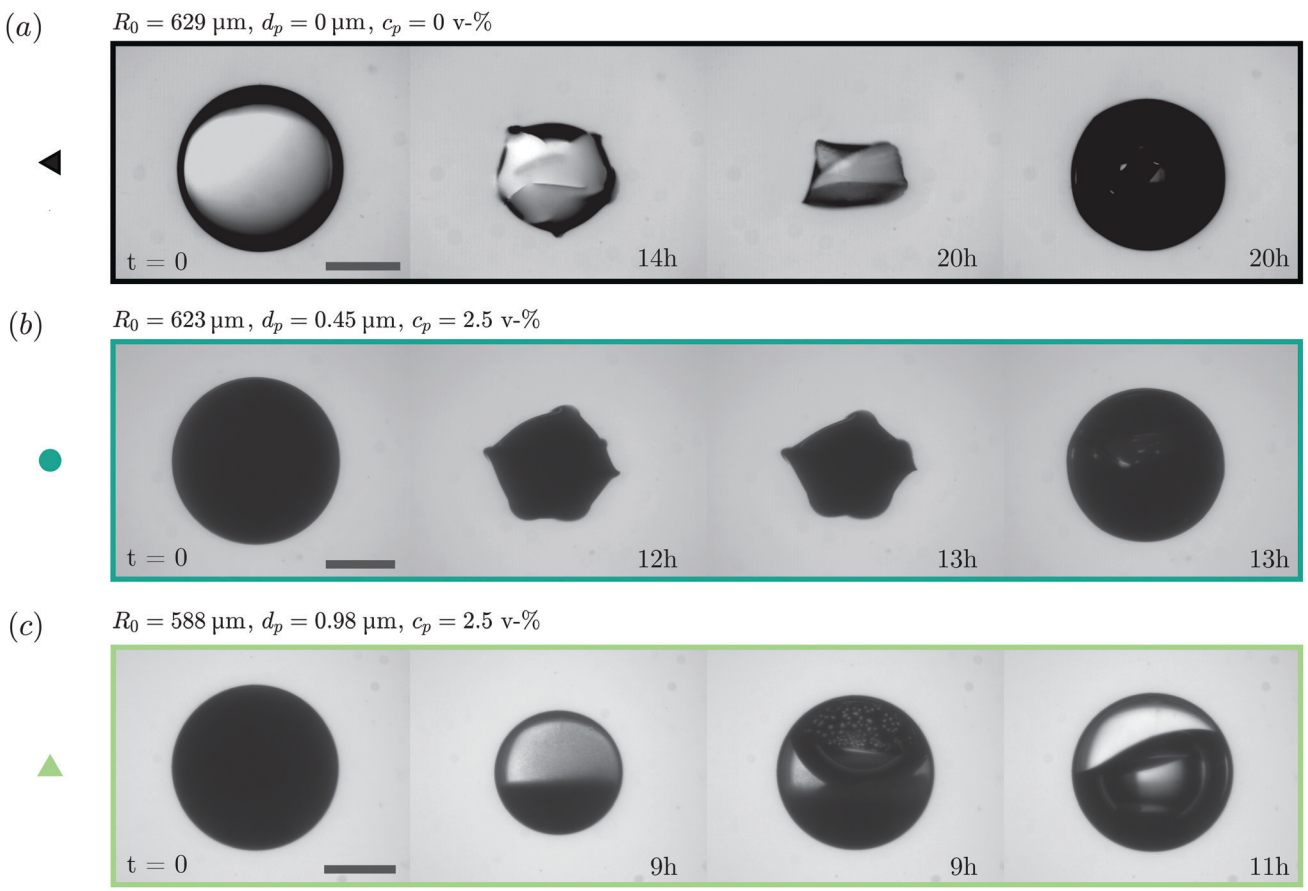

Fig. 3 The evaporation process for a droplet inside an elastic medium with and without particles. These three series correspond to the evaporation curves in Fig. 2. In figures (a) and (b) creasing and cavitation occurs, respectively without and with (small) particles. In (c) larger particles are used and creasing is no longer observed, only the cavitation event. The first image everywhere is the initial droplet, the third image is the last image before cavitation. In all series the scale bar represents 500 μm.

the three curves shown in Fig. 2 with matching colours and markers. Fig. 3a is an image sequence for the pure water experiment: first the droplet shrinks isotropically, then creasing occurs, and after some time the droplet experiences cavitation. A bubble nucleates and grows, ending up with practically the same size as the initial droplet. For more details on the cavitation dynamics we refer to ref. 12. In Fig. 3b a high concentration of small particles is added to the droplet (d_p = 0.45 μm, c_p = 2.5 v%). Clearly the droplet is no longer transparent, and appears opaque throughout the full experiment. Still, the creasing looks similar as to the case without particles and eventually also cavitation occurs. Fig. 3c shows the situation when the particle diameter is doubled (d_p = 0.98 μm, c_p = 2.5 v%), which also shows an opaque droplet due to the high particle concentration of that specific case. Due to their larger size, these particles start to sediment and a clear inhomogeneous particle distribution in the droplet is observed. The possible role of such an inhomogeneous particle distribution is unclear to us, but it will be nevertheless discussed below. Before creasing starts, a cavitation event occurs and the final bubble size has the same size as the initial droplet.

To analyse when creasing can be suppressed and early cavitation occurs, we performed a systematic study with different initial droplet radii, two different particle sizes and three particle concentrations. For each experiment we measure the radius at which cavitation occurs. These results are given in Fig. 4 for pure water droplets (Fig. 4a) and for two different particle sizes (Fig. 4b and c). On each subplot, for a given R_0, every droplet evolves from the top ($R(t)/R_0$ = 1) towards the

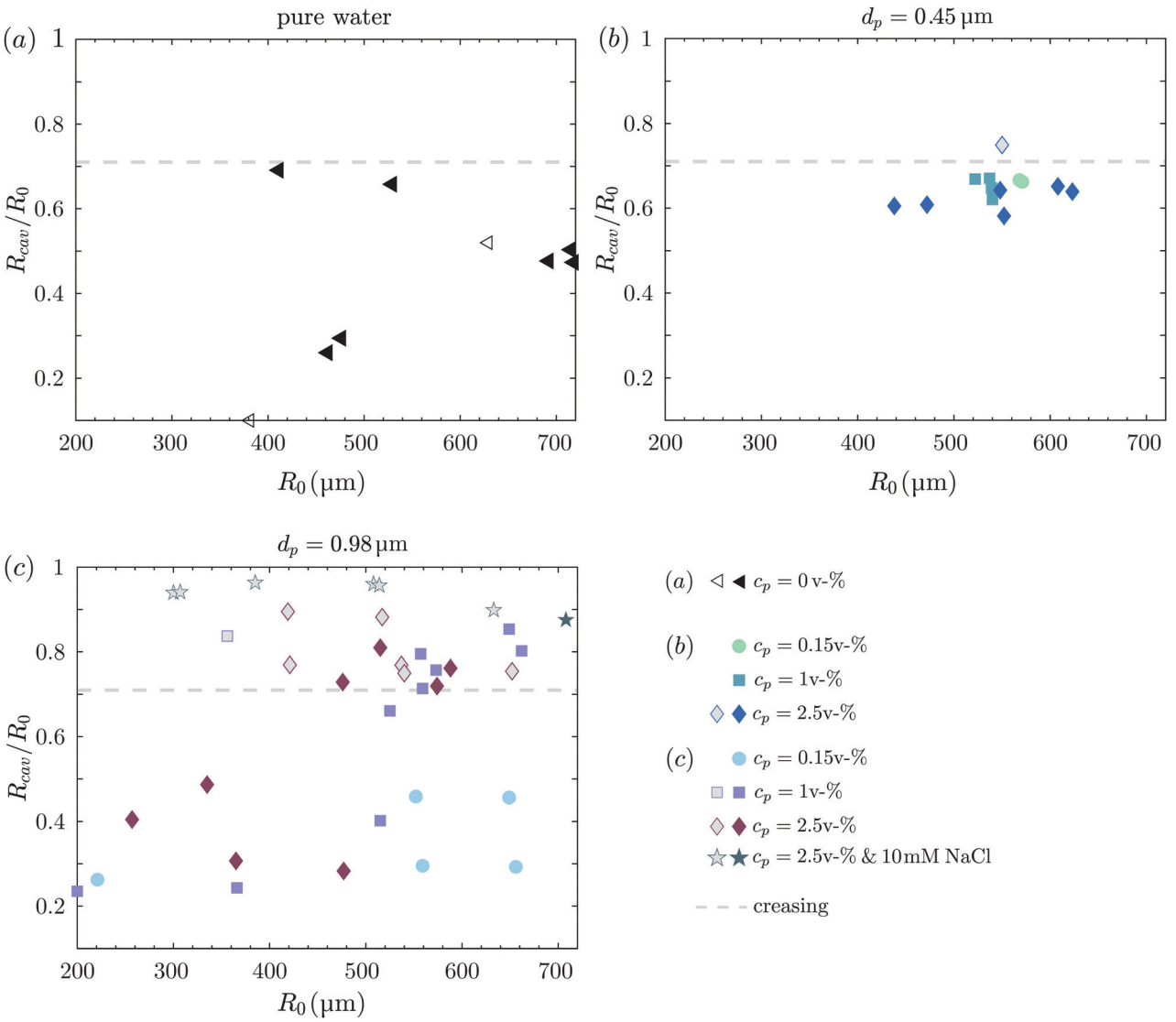

Fig. 4 The radius ratio at which cavitation occurs as a function of the initial droplet radius R_0 for different particle concentrations. Figures (a), (b) and (c) show the results for pure water droplets, d_p = 0.45 μm and 0.98 μm respectively. The radius ratio at which creasing occurs is highlighted with a grey dashed line. The grey markers are experiments in which cavitation type B is observed, the shape of the marker represents c_p. In figure (a) the open markers are results from the current study, the closed markers are from ref. 12. In figure (c) also experiments are included in which salt is added to the colloidal droplet, represented by star markers.

bottom of the graph, decreasing in size. The droplet will either crease when crossing the creasing radius ratio $R_{crease}/R_0 = 0.71$ (plotted as a grey dotted line), or it will go through a cavitation event before reaching the creasing line. Consequently, every point above the dotted line represents an experiment in which cavitation has occurred before creasing (early cavitation, *i.e.* $R_{cav}/R_0 > 0.71$). In the case of pure water droplets (Fig. 4a) cavitation is always observed for $R_{cav}/R_0 < 0.71$, meaning that creasing occurs for every experiment. Note that we are combining in this figure results from pure water droplets taken from ref. 12 and new measurements taken for this work. Surprisingly, the addition of a substantial amount of 0.45 μm-diameter particles does not change the process qualitatively: Almost all experiments experience creasing in a similar fashion as with pure water. A noticeable difference with pure water is that the cavitation events occur at similar radius ratios, closer to the creasing ratio, unlike the larger spread of the events for pure water.

Increasing the particle size to $d_p = 0.98$ μm has a significant effect, shown in Fig. 4c. In this graph we show the outcome for three different volume concentrations. For the lowest volume concentration ($c_p = 0.15$ v%), nothing different occurs compared to the previous results shown and the elastic medium always creases in the measured range of droplet sizes. However, increasing the particle concentration to $c_p = 1$ v%, results in a completely different behaviour. For droplets with R_0 larger than a certain critical radius R^*, cavitation occurs first, suppressing creasing completely, as already introduced in Fig. 3c. For an even higher particle concentration (2.5 v%), this critical radius shifts to a lower value. In summary, approximately half of the droplets containing larger particle concentrations experienced early cavitation, with a clear correlation on the initial droplet size R_0.

Using the results from Fig. 4 we can determine the critical radius R^* for each particle size and concentration. In the case of the 0.45 μm-diameter particles, no critical radius can be extracted from the range of measured R_0. For the case of 0.98 μm-diameter particles, an increase on the particle concentration is reflected in a decrease of R^*. We elaborate on the exact values of R^* in Fig. 6. Interestingly, droplets with $R_0 < R^*$ behave very similarly as pure water droplets: Starting with an isotropic shrinking of the droplet, continuing with a creasing instability at the expected radius ratio and eventually cavitation kicks in. However, in the case of $R_0 > R^*$, the process turns more complex. Experiments with 0.98 μm-diameter particles have shown two different kinds of cavitation events, both shown in Fig. 5. In the most common type found, which we will call type A (Fig. 5a), a bubble is nucleated at the very top of the droplet, apparently very close to the interface, it quickly loses its spherical shape and then sinks down. From there, it grows in time until the full droplet is evaporated and a bubble with the same size as the initial droplet is obtained. Although we lack more detailed observations to support this hypothesis, it seems as if this kind of bubble nucleation occurs at the PDMS–liquid interface, and therefore the bubble loses easily its sphericity. The fact that the bubble moves downwards, in the direction of gravity, is a puzzling observation. This motion must be driven by certain convection inside the drop following the bubble nucleation, but we are uncertain of its nature. Cavitation type A can be observed before and after creasing in suspension droplets with 0.98 μm-diameter particles, and only after creasing for 0.45 μm-diameter particles and pure water.

The second kind of cavitation, which we will call type B (Fig. 5b), has several interesting features. The bubble nucleates also in the upper part of the droplet, but it seems to be formed in the liquid bulk, as it retains its spherical shape during the

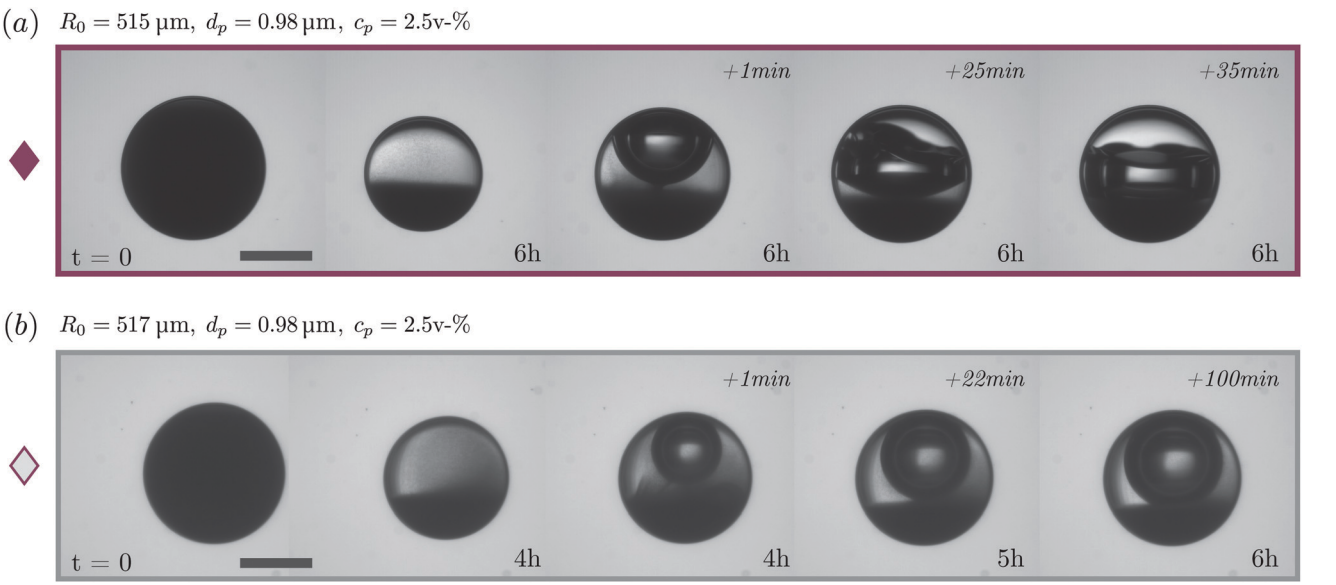

Fig. 5 Two types of cavitation for nearly identical initial conditions. The time scales in the upper right corner show the time after the cavitation bubble is formed. (a) Cavitation type A: a bubble is formed at the top of the droplet and then moves towards the bottom of the droplet. (b) Cavitation type B: a bubble is formed at the top of the droplet and remains at this location. The scale bars represents 500 μm and the same markers are used as in Fig. 4 and 6.

whole process of growth. Cavitation type B events are plotted using grey markers in all upcoming plots, from Fig. 4–10. It is important to stress that the difference between these two types of cavitation events is not only qualitative and visual (and therefore less objective), but also quantitative: all type B events in the presence of particles occurs before creasing. Note that a critical radius cannot be defined in this case since all cavitation type B events occur before creasing. The precise mechanism that allows the bubble to remain in place is for the moment unknown to us. In principle, by invoking symmetry, one would expect that the nucleation of a bubble at the liquid–gel interface, as seems to be the case in type A, would lead to much stronger flow than a bubble nucleating in the bulk. Another important observation from Fig. 4 and 5 is that for identical initial conditions, both types of cavitation are equally likely to occur. The experiments in Fig. 5a and b are performed with the same R_0, d_p and c_p.

To summarize the observations from Fig. 4, we make use of the resulting values for R^*. Fig. 6 shows the same data plotted as a phase diagram with the particle concentration c_p *versus* the initial droplet radius R_0. For each set of experiments we highlight if creasing can be suppressed or not. The colored regions are regions in which creasing is observed and cavitation occurs afterwards, *i.e.* $R_0 < R^*$. The non-colored bars show the conditions in which creasing can be suppressed and cavitation occurs early. For example, in the case of d_p = 0.98 μm and c_p = 2.5 v%, R^* is determined from two experiments at $R_0 \approx 477$ μm for which we observe creasing in one case and early cavitation in the other, so this radius represents the critical radius for this transition. In this phase space the experiments that displayed type B cavitation are also included in grey to ensure a complete overview. Once more, this figure highlights the unpredictable nature of the cavitation events: in Fig. 6a we can observe events of type A and B both occurring under almost identical conditions R_0 = 550 μm and c_p = 2.5 v% (for d_p = 0.45 μm); or in Fig. 6b, with R_0 = 356 μm and c_p = 1 v% (for d_p = 0.98 μm). Type B cavitation can occur both for $R_0 < R^*$ and $R_0 > R^*$. Opposed to this random occurrence of type B, type A cavitation never occurs for $R_0 < R^*$ and is therefore more reproducible and independent on the initial droplet radius.

3.2.1 Origins for the threshold to suppress creasing

3.2.1.1 Area of particles. In order to understand the origin for the observed critical radius R^*, which is a function of particles size and concentration, there are several factors to consider. Firstly, the reason for early cavitation must relate to the presence of particles in the system, as it is never observed in the case of pure water droplets (see Fig. 4a). The particles introduce an additional solid area into the system which might increase the amount of potential cavitation nuclei. These experiments have been categorised by their volume concentration c_p and initial droplet radius R_0. Following this hypothesis, the area of the particles inside the droplet should be the determining parameter and not their occupied volume or their number. In order to test this hypothesis, we calculate the total area of particles inside the droplet A_{tot}, using the volume concentration of particles, their size and the initial drop volume. The resulting phase space with c_p *versus* A_{tot} is shown in Fig. 7. Firstly, we observe that the measured range of A_{tot} is similar for the 0.45 and the 0.98 μm-diameter particles (Fig. 7a and b). This is not trivial, as the number of particles present in the droplet differs 1 order of magnitude: $N = \mathcal{O}(10^8)$ for 0.45 μm-diameter particles and $N = \mathcal{O}(10^7)$ for 0.98 μm-diameter particles (both for c_p = 2.5 v%). However, when the total area of the particles is calculated, such a difference vanishes, and in both cases we find $A_{tot} = \mathcal{O}(10^{-4})$ m^2. This tells us that the available area for nucleation alone is not sufficient to explain the occurrence of early cavitation only in the case of 0.98 μm-diameter

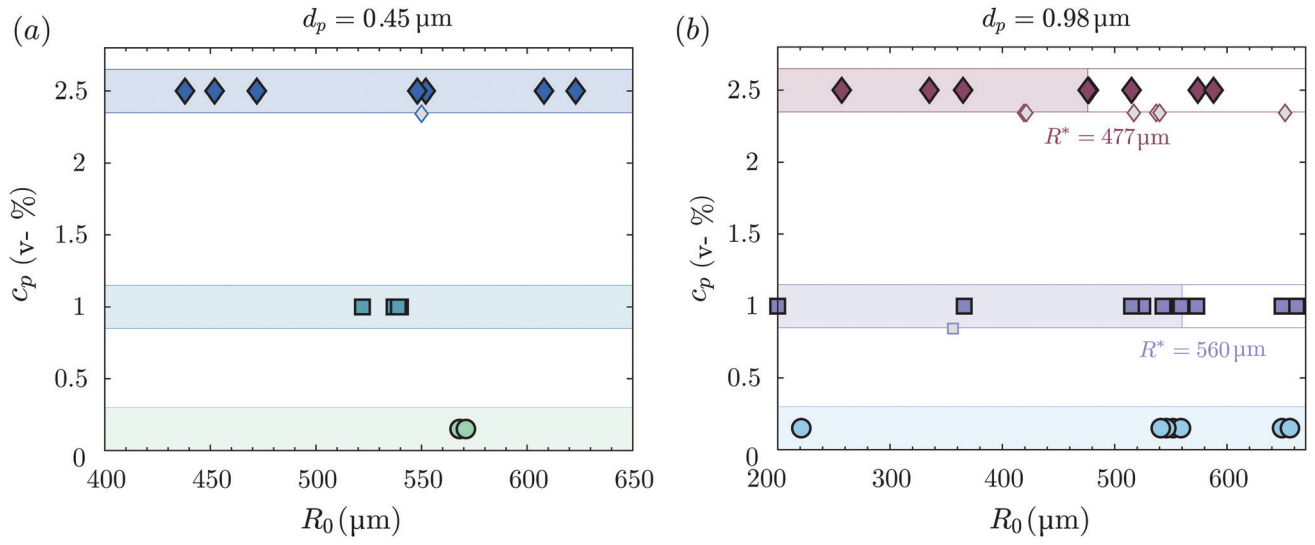

Fig. 6 Transition for suppressing creasing as a function of initial droplet radius R_0 and particle concentration, for two different particle sizes. In (a) and (b) the colored region represent the parametric region where creasing is observed (*i.e.* region where $R_0 < R^*$). In (b) the non-coloured bar represents the region in which $R_0 > R^*$: for these conditions creasing is suppressed and cavitation occurs early (type A cavitation). The grey markers are experiments in which type B cavitation is observed. Note that they are slightly shifted downwards in the *y*-axis only for clarity.

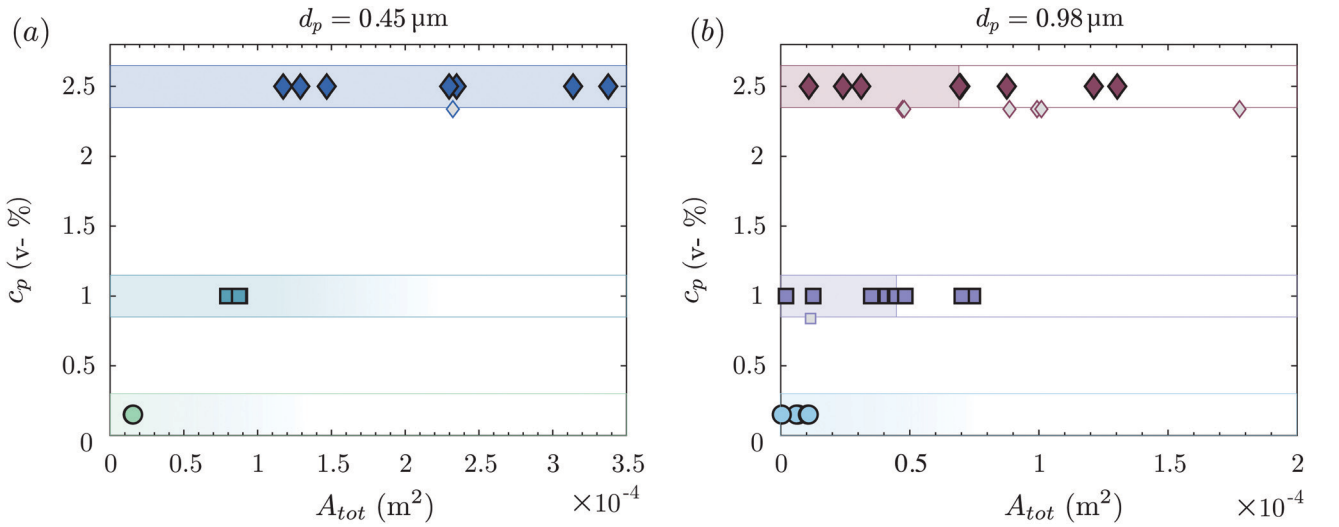

Fig. 7 Transition for suppressing creasing as a function of total area of all particles, for two different particle sizes. The colored bars show for each particle concentration where creasing is observed. In figure (b) also non-coloured bar are included: for these conditions creasing is suppressed and cavitation occurs early. For low particle concentrations in (a) and (b) the transition cannot be determined from the available experiments and therefore a fading color bar is used. The grey markers are experiments in which type B cavitation is observed.

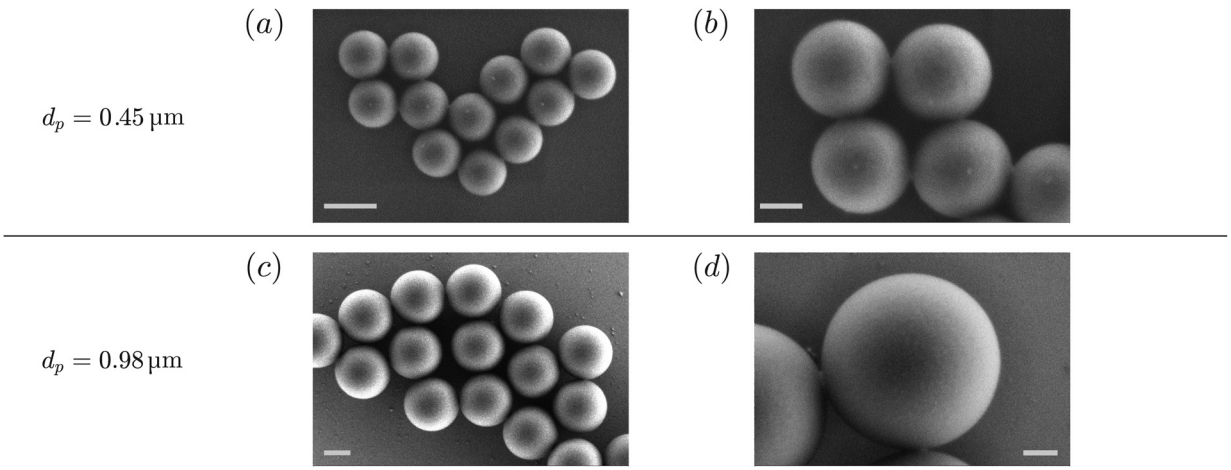

Fig. 8 Scanning electron microscope images from polystyrene particles (MicroParticles GmbH, PS-FluoRed). Figures (a) and (b) show two different magnifications for d_p = 0.45 μm. Figures (c) and (d) show two magnification levels for d_p = 0.98 μm. The scale bars in figures (a) and (c) represent 500 nm, in figures (b) and (d) 200 nm.

particles. For the smallest particle size in our set we are nearly never able to suppress creasing, even though the total available area is even slightly larger than in the case of the larger particles.

3.2.1.2 Roughness of particles. As mentioned in both Borkent *et al.*[13] and Marschall *et al.*,[17] the surface roughness of the immersed particles played an important role in increasing the cavitation activity in those experiments. In our case, both the 0.45 and 0.98 μm-diameter particles are produced by MicroParticles GmbH, they are made of polystyrene and are functionalized with sulfate groups. To ensure that the surface roughness is similar for the two types of particles, their surface has been analyzed using Scanning Electron Microscopy (SEM). Fig. 8 shows the surface of the particles for different magnifications. The polystyrene particles are difficult to image perfectly due to their non-conducting character. However, the SEM images show that, on a qualitative level, there is no significant difference between the roughness of these two types of particles that could explain the high contrasting results obtained for each of them.

3.2.1.3 Tensile strength. To gain more insight on the influence of particles on the cavitation process inside the droplet, the tensile strength is calculated from the cavitation events in each of our experiments. We define the tensile strength of our liquid solution as the pressure deficit necessary to cause a cavitation event. In our case, we will define the pressure deficit in the droplet at the moment of the cavitation event from the experimentally obtained curves for radius *versus* time. We use the elastic energy for a spherical cavity inside an elastic medium, which can be written as $\varepsilon_{el} = 4\pi\mu R_0^3 f(\zeta)$, where μ is the shear modulus of the surrounding elastic medium

(PDMS), and $\xi = R/R_0$. For a Neo–Hookean solid the dimensionless function reads $f(\xi) = \frac{5}{6}\xi^3 - \xi^2 - \frac{1}{3} + \frac{1}{2\xi}$.[22,23] The (negative) pressure of the droplet can be calculated using

$$P_{cav} = P_\infty + \frac{2\gamma}{R} + \frac{\mu}{\xi^2} f'(\xi), \quad (7)$$

where p_∞ is the atmospheric pressure far away from the droplet and γ is the surface tension of the water–PDMS interface. To calculate the critical tension for cavitation *i.e.* the tensile strength, in the case of the evaporation of colloidal droplets, we need to separate two different cases. When the presence of particles leads to the suppression of creasing, the droplet is still spherical while cavitating. For these measurements, we can insert the exact value of R_{cav}/R_0 for ξ and calculate the corresponding tensions. For example, the experiment with R_0 = 588 μm and c_p = 2.5 v% for the 0.98 μm-diameter particle. In this case ξ = 0.76, which results in P_{cav} = −1 MPa. Therefore the critical tension in the water droplet for cavitation is ∼1 MPa for early cavitation (type A or B). However, in experiments in which creasing occurs before cavitation, the value of ξ is not trivial. At the moment of creasing, the droplet looses its spherical cape and at the same time, the gel releases some of its build up tension. Therefore we use ξ at the moment of creasing (≈0.71) and the resulting pressure can be seen as a lower bound for the pressure upon which cavitation occurs. A typical value of P_{cav} = −1.5 MPa is obtained for ξ = 0.71, meaning that the critical tension for cavitation is ∼1.5 MPa in the case of creasing.

In Fig. 9 we summarise all results for the critical tension for the performed experiments. Fig. 9a contains the results for pure water and d_p = 0.45 μm. The critical tension for cavitation is ∼1.5 MPa for most of the experiments, as creasing occurs always before cavitation. All experiments in which creasing takes place are given with open symbols. As creasing always occurs near ξ = 0.71, the spread in this data is marginal and T_{cav} = 1.5 MPa. Only one experiment with 0.45 μm-diameter particles shows a tensile strength at substantially lower values than the rest, which interestingly corresponds cavitation type B, this is, with a bubble being apparently nucleated at the bulk. Fig. 9b shows the results for 0.98 μm-diameter particles, which make a stark contrast with those of pure water and 0.45 μm-diameter particles. The main difference is the significant amount of experiments showing tensile strengths below the creasing limit. Interestingly, there is a clear inverse correlation between the particle concentration and the tensile strength T_{cav}. Also note the large spread in tensile strength in the case of early cavitation (either type A or B) in comparison to the values obtained for pure water and 0.45 μm-diameter particles in Fig. 9a. In Fig. 9b, the only two values of T_{cav} observed above the creasing limit deserve a comment: These two points correspond to very low R_0 values (≈ 200 μm). A smaller initial droplet size involves a shorter life, which becomes somewhat comparable with the gel curing time. As a result, the creasing occurs at an effectively lower value of ξ, which leads

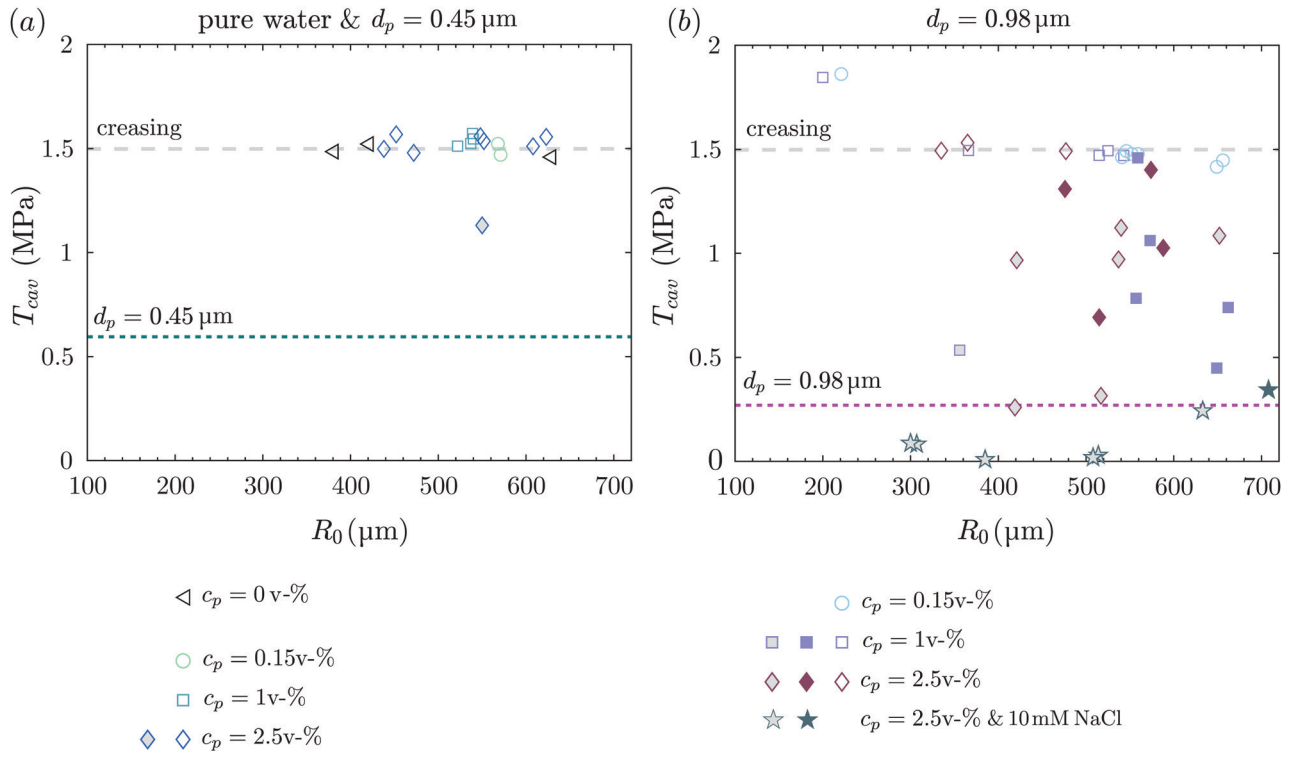

Fig. 9 The critical tension for cavitation for suspensions with different particle concentrations and sizes. The open markers highlight cases in which creasing occurs. The filled symbols represent type A cavitation, the grey markers the type B cavitation. Figure (a) shows the critical tension for d_p = 0.45 μm and pure water, figure (b) shows the results for d_p = 0.98 μm. The coloured dotted lines show the curves for $T_{cav} = 4\gamma/d_p$, the grey dashed line the critical tension in the case of creasing.

to a higher T_{cav}. For larger droplets this effect becomes negligible as the time it takes to evaporate the droplet is larger, whereas the time it takes for the gel to cure remains the same.

Marschall *et al.*[17] proposed that, in the case of smooth particles, the smallest possible tensile strength of a suspension is determined by the radius of curvature of the particle. The critical tension for cavitation is determined from the stress that needs to overcome the surface tension force of the vapour cavity with typical particle diameter d_p. This tension is expressed as $T_{cav} = 4\gamma/d_p$. The surface tension of the water–air interface is temperature dependent. As the plate is kept at 70 °C (corresponding to 64 mN m^{-1} [24]), but the surroundings are measured to be 40 °C (70 mN m^{-1} [24]), we have used an intermediate value of 67 mN m^{-1}. However, this range of values for γ only slightly influences the resulting value for T_{cav}. Note that the presence of particles should not have any effect on the value for γ, since the solutions are surfactant-free and the particles are fully hydrophilic.

The size of the particles is used as a typical length scale, as the vapour cavity with initial size d_p will detach from the solid surface and grow. We calculate this pressure for the two particle sizes which are studied. These theoretical bounds for the critical tension are also near 1 MPa and are given in Fig. 9a and b as dotted lines. The comparison of this theoretical bound with our experimental data becomes particularly interesting for the 0.98 μm-diameter particles in Fig. 9b. Most of the data lies in between the creasing limit and the single-particle theoretical bound represented by the dotted line. However, in Fig. 9a (d_p = 0.45 μm) the values for the tensile strength are larger than the theoretically predicted by the particle size. According to the predictions of Marschall *et al.*,[17] the tensile strengths found correspond approximately to the radius of the particles (see Fig. 10) and correspond to the same order of magnitude. Therefore, we do not expect that roughness at the particles surface in the nanometric range would play a significant role as nano-crevices in our experiments.

The results shown above indicate the existence of nucleation sites smaller than the particle diameter. It would be therefore interesting to alter the length scale of the potential nucleation sites in the droplets. On the one hand, using smaller particles than d_p = 0.45 μm would not give additional information, since the results have been quite insensitive to their presence. On the other hand, larger particles than d_p = 0.98 μm would enhance the sedimentation of the particles to the bottom of the droplets, which involves complex additional effects. Instead, we performed series of experiments with 0.98 μm-diameter particles adding a small amount of sodium chloride to the particle solution. The presence of ions in the solution increases the screening of the electrostatic barrier that prevents the particles from aggregation,[25] and therefore we expect to promote the presence of clusters, which would introduce a spread in the effective size distribution of the particles in solution. We add 10 mM NaCl to the particle solution, which is far below the saturation concentration of NaCl (roughly 6 M), and therefore we do not expect crystallisation to influence the evaporation of the droplet.

According to the argument introduced above, and in line with several ref. 13, 14 and 17, the presence of salt promotes the formation of particle clusters, which would decrease the critical pressure for cavitation, *i.e.* T_{cav} should decrease. This is precisely the effect observed in the experiments with salt, which are shown as star markers in Fig. 4 and in Fig. 9b. Fig. 4 clearly shows that the droplets containing salt and 0.98 μm-diameter particles cavitate in a very early stage (large R_{cav}/R_0), when only a small amount of elastic tension has built up in the droplet.

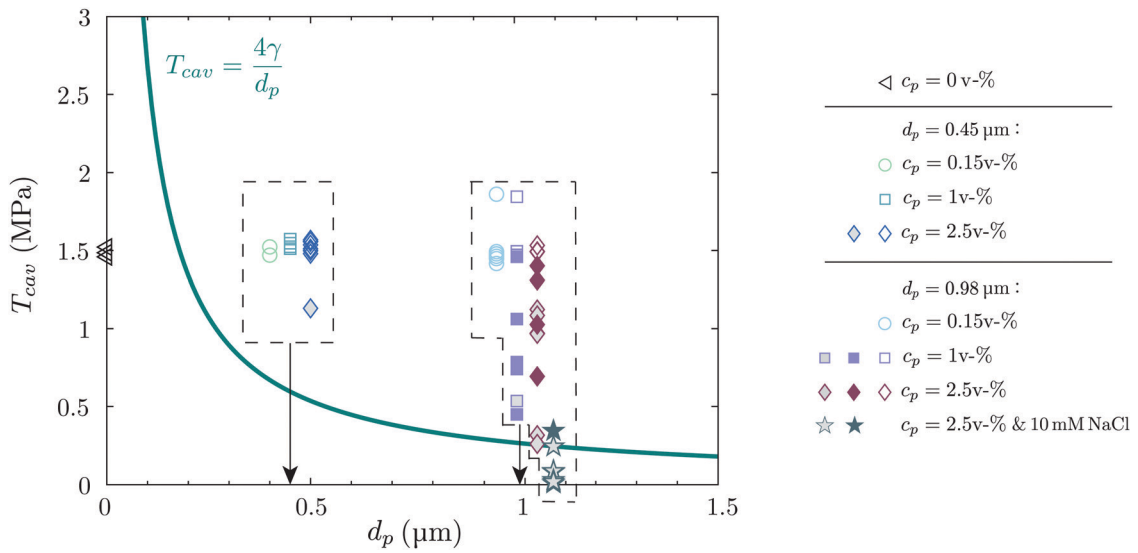

Fig. 10 The tensile strength of water that contains different particle concentrations and particle sizes. The open markers highlight cases in which creasing occurs. The filled symbols represent the type A cavitation experiments, the grey markers represent type B cavitation. Experiments without any particles inside the droplet are shown as black triangles at d_p = 0. Also experiments containing salt are included, represented by star markers. The individual data sets at d_p = 0.45 and 0.98 μm are shifted slightly apart from each other, for clarity. The solid line shows the curve for $T_{cav} = 4\gamma/d_p$.

Consequently, Fig. 9b shows that the critical tension for cavitation clearly decreases when compared to the situation without salt, and even reaches values below the predicted curve for d_p = 0.98 μm. This means that the typical length associated to the critical stress from the surface tension is in this case larger than the particle diameter itself. Also interesting is the fact that most of the cavitation events observed in the presence of salt are of type B. We hypothesized above that type B cavitation events seem to take place in the liquid bulk due to the presence of particles, and this observation goes in the line of our hypothesis.

4 Conclusions

In this work, we have studied how the presence of colloidal particles alters the occurrence of cavitation and creasing in a shrinking droplet under elastic tension in a PDMS gel. Surprisingly, 0.45 μm-diameter particles do not seem to influence the cavitation whatsoever, only in a marginal statistical proportion of the experiments performed. On the contrary, the influence of 0.98 μm-diameter particles is considerable. Cavitation events occur often before any creasing develops and the chances of this to occur are proportional to the particle concentration. Our main conclusion is that the onset of cavitation is largely influenced by the length scale of the particles or by their cluster size, as has been confirmed by introducing salt into the droplets to promote particle clustering. However, several questions remain open. One of the most important unanswered questions is the stark contrast between the 0.45 μm-diameter and the 0.98 μm-diameter particles; the former shows no influence from the particles and the later does, but the influence comes from unknown length scales in between the particle diameter and the creasing limit. Furthermore, the exact origin for the existence of the critical droplet radius R^* (above which no creasing is observed) is still an open question. Several routes could be explored to gain more insight into the influence of particles on the onset of cavitation, using particles with different surface roughness or different wetting properties. This could also lead to a deeper understanding of the two different types of cavitation which are observed. Consequently, predictions could be obtained on how the initial droplet size, particle size and/or particle concentration influence the outset of cavitation, not only in our system, but also on related systems with particle solutions under tension. The occurrence of cavitation at the upper part of the droplet is also intriguing. Although sedimentation of particles towards the bottom of the droplet is clearly noticeable in our experiments (see for example Fig. 5), bubbles always nucleate at the upper part of the droplet, *i.e.* at the location of lowest particle concentration. This at first counter-intuitive observation may be explained with the ability of some particle to trap gaseous nuclei together with the long time-span of hours to build up tension. Single particles or agglomerates of particles trapping gaseous nuclei would be more buoyant than fully wetted particles with a density of ρ = 1.05 kg m^{-3}. Because the present particles' density is very close to the density of water, already a small amount of gas trapped could render them buoyant and accumulate these at the upper part of the droplet. If this would be the case, particles trapping more gas (most buoyant) would be located at the upper part of the droplet, while the rest would sediment to the droplet's lower part. This resulting stratification of buoyant particles at the top and particles without gas entrapment at the base may explain why the nucleation event occurs always on the top of the droplet.

Our experimental results show that fairly smooth particles with diameters in the order of 0.5 μm do not stimulate cavitation events in evaporating droplets within an elastic matrix, while those in the order of 1 μm do. This result should be independent on the nature or rheology of the matrix itself, and therefore it is an interesting conclusion both for practical applications as for rigid-walled cells exposed to such stresses.[7]

In addition, our experimental system has shown to be a very reliable system to study the onset of cavitation in soft and elastic systems. The tensile strength of the solution can be measured through a rather simple preparation. By varying the elastic modulus of PDMS (*e.g.* mixing ratio during preparation) different regions of tensile strength can be probed. This would be of special interest for the characterization of solutions with particles that operate as sub-micrometric cavitation nucleation agents, promoting drug distribution and improving therapeutic efficacy in the body.[26] Additionally, the onset of cavitation before creasing could be an interesting advantage to introduce perfectly spherical bubbles in a controlled manner for the fabrication of soft acoustic metamaterials.[27] To conclude, we believe that the phenomena here described is a particular good example of the multifaceted puzzles that bubbles often manifest.[28,29]

Conflicts of interest

There are no conflicts to declare.

Acknowledgements

MB and AM acknowledge financial support from the European Research Council, ERC-StG-2015 NanoPacks, Grant agreement No. 678573. The authors thank Mark Smithers from the MESA+ Nanolab for his technical assistance with the Scanning Electron Microscope.

Notes and references

1 R. Rizzieri, L. Mahadevan, A. Vaziri and A. Donald, *Langmuir*, 2006, **22**, 3622–3626.
2 M. P. Milner, L. Jin and S. B. Hutchens, *Soft Matter*, 2017, **13**, 6894–6904.
3 A. A. Evans, E. Cheung, K. D. Nyberg and A. C. Rowat, *Soft Matter*, 2017, **13**, 1056–1062.
4 B. Lynch, C. Bonod-Bidaud, G. Ducourthial, J. S. Affagard, S. Bancelin, S. Psilodimitrakopoulos, F. Ruggiero, J. M. Allain and M. C. Schanne-Klein, *Sci. Rep.*, 2017, **7**, 1–10.
5 Q. Zheng, D. Durben, G. Wolf and C. Angell, *Science*, 1991, **254**, 829–832.

6 D. Or and M. Tuller, *Water Resour. Res.*, 2002, **38**, 19–21.
7 L. L. Vergeynst, M. G. Sause, N. J. De Baerdemaeker, L. De Roo and K. Steppe, *Tree Physiol.*, 2016, **36**, 786–796.
8 X. Noblin, N. O. Rojas, J. Westbrook, C. Llorens, M. Argentina and J. Dumais, *Science*, 2012, **335**, 1322.
9 O. Vincent, P. Marmottant, P. A. Quinto-Su and C. D. Ohl, *Phys. Rev. Lett.*, 2012, **108**, 184502.
10 O. Vincent, P. Marmottant, S. R. Gonzalez-Avila, K. Ando and C. D. Ohl, *Soft Matter*, 2014, **10**, 1455–1458.
11 B. Dollet, P. Marmottant and V. Garbin, *Annu. Rev. Fluid Mech.*, 2019, **51**, 331–355.
12 M. A. Bruning, M. Costalonga, J. H. Snoeijer and A. Marin, *Phys. Rev. Lett.*, 2019, **123**, 214501.
13 B. M. Borkent, M. Arora and C. D. Ohl, *J. Acoust. Soc. Am.*, 2007, **121**, 1406–1412.
14 A. A. Atchley and A. Prosperetti, *J. Acoust. Soc. Am.*, 1989, **86**, 1065–1084.
15 J. Rodríguez-Rodríguez, A. Casado-Chacón and D. Fuster, *Phys. Rev. Lett.*, 2014, **113**, 214501.
16 P. Vega-Martnez, O. R. Enrquez and J. Rodrguez-Rodrguez, *Beverages*, 2017, **3**, 38.
17 H. B. Marschall, K. A. Mørch, A. P. Keller and M. Kjeldsen, *Phys. Fluids*, 2003, **15**, 545–553.
18 C. Llorens, M. Argentina, N. Rojas, J. Westbrook, J. Dumais and X. Noblin, *J. R. Soc., Interface*, 2016, **13**, 20150930.
19 H. Gelderblom, A. G. Marin, H. Nair, A. Houselt, L. Lefferts, J. H. Snoeijer and D. Lohse, *Phys. Rev. E: Stat. Phys., Plasmas, Fluids, Relat. Interdiscip. Top.*, 2011, **83**, 026306.
20 S. J. Harley, E. A. Glascoe and R. S. Maxwell, *J. Phys. Chem. B*, 2012, **116**, 14183–14190.
21 G. C. Randall and P. S. Doyle, *Proc. Natl. Acad. Sci. U. S. A.*, 2005, **102**, 10813–10818.
22 A. N. Gent and C. Wang, *J. Mater. Sci.*, 1991, **26**, 3392–3395.
23 A. N. Gent and P. B. Lindley, *Proc. R. Soc. London, Ser. A*, 1959, **249**, 195 LP–205 LP.
24 J. Kwan, *CRC Handbook of Chemistry and Physics*, CRC Press, 101st edn, 2020.
25 R. J. Hunter, *Foundations of Colloid Science*, Oxford University Press, 1987.
26 J. J. Kwan, G. Lajoinie, E. P. Stride, M. Versluis and C. Coussios, *J. Acoust. Soc. Am.*, 2018, **143**, 1834.
27 T. Brunet, J. Leng and O. Mondain-Monval, *Science*, 2013, **342**, 323–324.
28 D. Lohse, *Phys. Today*, 2003, **56**, 36.
29 D. Lohse, *Phys. Rev. Fluids*, 2018, **3**, 110504.